Neuropeptide Y Y$_1$ receptor-mediated biodegradable photoluminescent nanobubbles as ultrasound contrast agents for targeted breast cancer imaging

CrossMark

Juan Li [a, 1], Yuchen Tian [a, b, 1], Dingying Shan [c], An Gong [a], Leyong Zeng [a], Wenzhi Ren [a], Lingchao Xiang [a], Ethan Gerhard [c], Jinshun Zhao [d], Jian Yang [c], Aiguo Wu [a, *]

[a] Key Laboratory of Magnetic Materials and Devices & Key Laboratory of Additive Manufacturing Materials of Zhejiang Province & Division of Functional Materials and Nanodevices, Ningbo Institute of Materials Technology and Engineering, Chinese Academy of Sciences, Ningbo 315201, PR China
[b] Nano Science and Technology Institute, University of Science and Technology of China, Suzhou 215123, PR China
[c] Department of Biomedical Engineering, Materials Research Institute, The Huck Institutes of the Life Sciences, The Pennsylvania State University, University Park, PA 16802, USA
[d] Public Health Department, Ningbo University, 818 Fenghua Road, Ningbo 315211, PR China

A R T I C L E   I N F O

A B S T R A C T

Targeted molecular imaging has attracted great attention in cancer diagnosis and treatment. However, most clinically used ultrasound contrast agents (UCAs) are non-targeted microbubbles seldom used for cancer imaging. Here, we fabricated fluorescent nanobubbles (NBs) by encapsulation of liquid tetradecafluorohexane (C_6F_{14}) within biodegradable photoluminescent polymers (BPLPs) through an emulsion-evaporation process and conjugation of PNBL-NPY ligand for specific targeting of Y$_1$ receptors overexpressed in breast tumors. The developed PNBL-NPY modified NBs were uniform in size with good dispersibility and photostability, presenting good ultrasound enhancement. Further, *in vitro* and *in vivo* results indicated that the fabricated NBs exhibit high affinity and specificity to Y$_1$ receptor-overexpressing breast cancer cells and tumors with minimal toxicity and damage to organs. Our developed PNBL-NPY-modified NBs are novel targeted UCAs for safe, efficient and specific targeted breast cancer imaging, and may provide a new nanoplatform for early cancer diagnosis and treatment in the future.

1. Introduction

Breast cancer has become the most commonly diagnosed cancer among women [1]. Early diagnosis and monitoring is critical to cancer treatment [2,3]. Contrast agents have generated a huge scientific and economic impact on a broad range of early cancer diagnoses [4]. Compared to commonly used magnetic resonance imaging (MRI), positron emission tomography (PET) and computed tomography (CT), ultrasound imaging is a widely available, non-invasive and cost-effective diagnostic modality. It provides real-time imaging without the use of hazardous ionizing radiation, but the weak difference in echogenicity between different tissues often hampers a clear diagnosis [5–7]. In order to better visualize specific tissues, microbubble (MB)-based ultrasound contrast agents (UCAs) are frequently used as blood pool agents with a typical diameter of 1–8 μm [8–10]. However, MBs cannot permeate through the tumor vasculature to the cellular target site to generate the desired diagnostic and therapeutic effect [9]. Therefore, researchers are paying more attention to developing nanobubble (NB)-based UCAs for tumor ultrasound imaging.

Recently, NBs with various gas, liquid or solid cores and shells composed of polymers, such as PLA or PLGA, have been applied in tumor ultrasound imaging [11–15]. It was shown that these constructs exhibit optimal contrast enhancement abilities due to the enhanced permeation and retention (EPR) effect, thus accomplishing passive targeting to tumors [13,16]. At the same time, improving the selectivity of contrast agents to the specific cancer cells has become the focus of many researchers. Active targeting molecules have attracted great attention for targeted molecule imaging systems such as MRI, PET and ultrasonography [7,17–19].

Historically, the application of active targeting molecules for breast cancer targeting has demonstrated limited success due to the low expression of their receptors in breast tumors, such as folate receptors (~29%) and integrin receptors (~26%) [20,21], or co-expression in the normal and tumor breast tissues, such as vaso-active intestinal peptide receptors and gastrin-releasing peptide receptors [22,23]. The application of such targeting molecules often results in significant off-target effects.

Excitingly, we have recently identified a selective ligand of neuropeptide Y Y_1 receptors (Y_1Rs), PNBL-NPY, which has demonstrated a high selectivity to breast cancer cells with no effects on the normal breast cells [24]. Y_1Rs are highly overexpressed in human breast tumors and metastases (above 90%), while the normal breast tissues express Y_2Rs only [25,26]. Therefore, the development of Y_1R-based contrast agents will provide safer and more specific imaging for breast cancer diagnosis. Until now, most of the studies related to Y_1Rs mainly focused on scintimammography or PET imaging for breast cancer; however, there are no previous studies about the application of Y_1R ligands in ultrasound imaging [27–31].

Recently, a family of biodegradable photoluminescent polymers (BPLPs) has been reported by Yang et al. [32–35]. The reactants used to synthesize BPLPs, including citric acid, amino acids and aliphatic diols, are common compounds used in many FDA-regulated devices [32]. In contrast to photobleaching organic dyes, cytotoxic quantum dots, and conventional non-degradable fluorescent polymers, BPLPs are intrinsically fluorescent without conjugating any additional organic dyes or quantum dots and have demonstrated excellent photostability, biocompatibility, and degradability [32,34]. By initiating the ring-opening polymerization of L-lactide and glycolide with BPLP-cysteine (BPLP-Cys), biodegradable photoluminescent poly-L-lactide (BPLP-PLLA) and poly(L-lactide-co-glycolide) (BPLP-PLGA) have recently been developed based on BPLPs [34,36]. The obtained polylactone materials can be conveniently used to fabricate nanoparticles for nanoparticle tracking with a variety of microscopy techniques including fluorescent microscopy, confocal laser scanning microscopy (CLSM) and two-photon microscopy [37].

This study aims to develop Y_1R-based intrinsically fluorescent NBs as contrast agents for targeted ultrasound imaging of breast cancer. BPLP-PLLA-Cys was used for the preparation of intrinsically fluorescent NBs with contrast-enhanced ultrasound mode function and *in vitro* fluorescent imaging with a high quantum yield (up to 51%). Afterwards, a selective Y_1R ligand, PNBL-NPY, was conjugated to the NBs for the specific targeted imaging of Y_1R-over expressing breast cancer cells. The developed PNBL-NPY modified NBs were characterized, and their targeting ability and ultrasound-enhancing ability to breast tumors, as well as the toxicity to organs, were investigated via carefully designed *in vitro* and *in vivo* experiments. We have demonstrated that these unique intrinsically fluorescent NBs exhibit excellent aqueous stability, photostability, low toxicity and high contrast enhancement ability, making them extremely promising UCAs for ultrasound imaging of Y_1R-overexpressing breast cancer.

2. Material and methods

2.1. Materials

BPLP-PLLA50-Cys was synthesized as previously described [34,36]. Dichloromethane, 1-ethyl-3-(3-dimethylaminopropyl) carbodiimide hydrochloride (EDAC) and *N*-hydroxysuccinimide (NHS) were purchased from Sinopharm Chemical Reagent Co., Ltd (Shanghai, China). Polyvinyl alcohol (PVA), sodium cholate hydrate, HPLC grade acetonitrile and trifluoroacetic acid (TFA) were purchased from Aladdin Industrial Inc (Shanghai, China). Dulbecco's Modified

Eagle Medium (DMEM), RPMI-1640 medium, fetal bovine serum (FBS), penicillin, streptomycin and rhodamine phalloidin (RP) were purchased from Invitrogen™ (Carlsbad, USA). Tetradecafluorohexane (C_6F_{14}) was purchased from Sigma-Aldrich Co. LLC (Shanghai, China). [Pro^{30}, Nle^{31}, Bpa^{32}, Leu^{34}]NPY(28—36) (Ile-Asn-Pro-Nle-Bpa-Arg-Leu-Arg-Try-NH$_2$) was synthesized by the LifeTein LLC (Beijing, China). 1, 2-distearoyl-sn-glycero-3-phosphoethanolamine-*N*-[carboxy(poly ethylene glycol)-2000] (DSPE-PEG-COOH) was purchased from A.V.T. Pharmaceutical Ltd. (Shanghai, China), and DiI was purchased from Beyotime Biotechnology (Haimen, China).

2.2. Preparation of intrinsically fluorescent BPLP-PLLA-Cys nanobubbles (BPC-NBs)

The intrinsically fluorescent BPC-NBs were prepared by modifying the solvent emulsion/evaporation method to obtain NBs with a polymeric shell encapsulating tetradecafluorohexane (C_6F_{14}) [13]. Briefly, 0.1 g BPC was dissolved into 4 mL dichloromethane containing 60 μL of C_6F_{14}. The mixture was ultrasonicated for 5 min at 600 W with an ultrasonic cleaner (SB 25-12DTDN, Ningbo Scientz Biotechnology Co., Ltd. China) to ensure full miscibility of the C_6F_{14}. Afterwards, the organic solution was added into 20 mL of 1.5% sodium cholate (w/v) aqueous solution, and then the mixture was emulsified by a superfine homogenizer (F6/10, FLUKO, China) operating with a 10 G dispersing tool (10 000 rpm, 1 min) to form a pre-emulsion. For *ex vivo* fluorescence imaging experiments, DiI was added to the organic solution prior to emulsification. Typically, about 10 μL a concentrated DiI solution (1.2 μg mL^{-1} in ethanol) was added to the organic solution.

The pre-emulsion was sonicated at 648 W with a vibrating metallic tip for 1 min. The organic solvent was then evaporated by magnetic stirring for 4 h at room temperature. After full evaporation of the solvents, the suspension volume was adjusted to 20 mL with water, and then incubated with 1.5% PVA (w/v) for 5 days at 4 °C to replace sodium cholate. The formed BPC-NBs were washed with distilled water by centrifugation (10,000 g, 1 h, 4 °C). The supernatant was discarded and the BPC-NBs were resuspended with 5 mL water for the subsequent experiment.

2.3. Conjugation of PNBL-NPY to the BPC-NBs

To conjugate the PNBL-NPY ligand onto the surface of BPC-NBs, an EDAC/NHS activation technique was used [24]. Before the conjugation, BPC-NBs were modified with DSPE-PEG-COOH. 1.0 mg mL^{-1} DSPE-PEG-COOH in ethanol was added to the BPC-NBs, and the ethanol was evaporated by magnetic stirring for 4 h at room temperature, followed by washing with distilled water via centrifugation (10,000 g, 1 h, 4 °C). The carboxylic groups of BPC-NBs were conjugated with the amine group of PNBL-NPY. Briefly, an ice cold mixture of 0.3 mL EDAC (0.3 mg mL^{-1} in PBS) and 0.2 mL NHS (0.3 mg mL^{-1} in PBS) was added into a 10 mL BPC-NB solution (1 mg mL^{-1} in PBS) under continuous stirring for 15 min (ice water bath). Then 1.0 mL PNBL-NPY solution (in PBS) with different concentrations were added dropwise into the above solution and reacted at room temperature for 16 h. The prepared BPC-NB-PNBL-NPY was centrifuged (14,000 g, 30 min) and the supernatants were stored for further analysis. Unreacted PNBL-NPY in the supernatant were quantified with a HPLC-UV method as previously described [24]. A simple mass balance was then used to calculate the amount of PNBL-NPY conjugation on the surface of BPC-NBs.

2.4. Characterization

A particle size-zeta potential analyzer (Nano-ZS, Malvern, England) was used for the measurement of particle size and zeta

potential of the BPC-NB-PNBL-NPY at room temperature. Results were expressed as the average of the mean diameter of the NBs obtained from three measurements. High-resolution transmission electron microscopy (HRTEM) images were recorded by a JEOL-2100 (JEOL, Japan) instrument to get detailed structural and morphological information of BPC-NB-PNBL-NPY. 3 μL of the BPC-NB-PNBL-NPY solution was dropped on a 300 mesh copper grid coated with a thin layer of carbon film, and another 2 μL of 0.5% phosphotungstic acid was dropped on top of the NB droplet for negative staining. The copper grid was dried overnight at room temperature before TEM analysis.

Photoluminescence spectra of BPC-NB-PNBL-NPY solutions were acquired on a Hitachi F-4600 fluorospectrophotometer (Hitachi, Japan). Both the excitation and the emission slit widths were set at 5 nm for all samples unless otherwise stated. The photostability of BPC-NB-PNBL-NPY solution was evaluated by recording the changes of the fluorescence intensity of the samples under continuous excitation in the fluorospectrophotometer. The excitation wavelength for photostability tests was determined by the maximum absorbance spectra of each type of sample.

2.5. Cell culture

Human breast cancer MCF-7 cell line and Mouse breast cancer 4T1 cell line were cultured in Dulbecco's modified Eagle's medium (DMEM) and RPMI-1640 medium respectively, and both of the medium were supplemented with 10 wt % fetal bovine serum (FBS), 100 units mL^{-1} of penicillin, and 100 mg mL^{-1} of streptomycin. The cells were maintained in a 37 °C incubator with 5% CO_2.

2.6. Cell viability assays

Cytotoxicity of NBs to the MCF-7 and 4T1 cells were measured by flow cytometry analysis. Both MCF-7 and 4T1 cells were treated with different concentrations of BPC-NB and BPC-NB-PNBL-NPY for 24 h. Cells were collected and stained by propidium iodide (PI) and analyzed by flow cytometry analysis immediately. The PI positive cells were recognized as dead cells [38]. 2.0 mL of MCF-7 (or 4T1 cells) in complete DMEM medium (or RPMI-1640 medium) were seeded into each well at 5×10^4 cells mL^{-1} and cultured overnight. On the following day, the culture media were replaced by fresh medium containing different concentrations of BPC-NB and BPC-NB-PNBL-NPY. After a further 24 h incubation, the cells were washed three times with 1 mL PBS to remove any absorbed free NBs and then harvested for further analysis. Cells were stained with propidium iodide (PI) for 5 min at room temperature. The mean fluorescence intensity (MFI) of cells (1×10^4 counts) were analyzed by flow cytometry (LSRFortessa, BD, USA), where the gate was arbitrarily set for the detection of PI (600—630 nm) with forward and side scattering dot plots used to discriminate cellular debris.

2.7. In vitro specific targeting of BPC-NB-PNBL-NPY

The ethanol treated glass slides were put in 6-well plates and coated with 0.01% poly-L-lysine. 2.0 mL of MCF-7 (or 4T1 cells) in complete DMEM medium (or RPMI-1640 medium) were seeded into each well at 5×10^4 cells mL^{-1} and cultured overnight. On the following day, the culture media were replaced by fresh medium with different treatments including 500 μg mL^{-1} BPC-NB, 500 μg mL^{-1} BPC-NB-PNBL-NPY, or PBS. After 12 h further incubation, the cells were washed three times with 1 mL PBS to remove any adsorbed free NBs. For LSCM imaging, the cells were fixed with 1 mL 4% formaldehyde for 30 min, then washed three times with 1 mL PBS. Cells were then treated with 1 mL 0.1% triton for 5 min, washed three times with 1 mL PBS and then treated with 1 mL 1.0%

BSA for 30 min at room temperature. The actin of the cells was stained with 200 μL rhodamine phalloidin (RP) for 30 min at room temperature. The samples were simultaneously excited at 405 and 540 nm and the fluorescent images at emission wavelengths 420—500 and 600—660 nm were observed by a LSCM (TCS SP5 II, Leica, Germany). For flow cytometry analysis, the mean fluorescence intensity (MFI) of cells (1×10^4 counts) was analyzed by flow cytometer (LSRFortessa, BD, USA), where the gate was arbitrarily set for the detection of blue fluorescence (425—475 nm) with forward and side scattering dot plots used to discriminate cellular debris.

2.8. In vitro ultrasound imaging

In vitro ultrasound imaging of BPC-NB-PNBL-NPY was carried out in a latex tube (inner diameter of 6 mm) which was embedded into 1% agarose gel as previously reported [10]. The NBs (5 mg mL^{-1} in PBS) were injected into the latex tube simulating the blood vessel and circulated in the tube with a constant flow rate controlled by a pump. Ultrasonography was performed using a M9DP-50 portable ultrasonic imaging system (Mindray, Shenzhen, China) in visualization mode with a transducer set to a frequency 10.0 MHz.

2.9. Animal models

Female Balb/c mice (18—20 g, 4—6 weeks old) were used in this work. All the experimental protocols involving animals were approved by the Regional Ethics Committee for Animal Experiments at Ningbo University (Permit No. SYXK Zhe 2013-0191). The tumor model of murian breast cancer was established by subcutaneous injection of 4T1 cells. Briefly, 4T1 cells (1×10^6 cells for one mouse) suspended in 100 μL of serum free medium were inoculated subcutaneously in several female Balb/c mice (five weeks old) at the back. A digital caliper was used to measure the tumor size. Tumors with a diameter of 0.8—1.2 cm were selected for subsequent experiments.

2.10. Toxicity evaluation in vivo

For *in vivo* toxicity, 24 healthy Balb/c mice were randomly divided into eight groups (3 each group), and were injected with BPC-NB-PNBL-NPY (50, 100 or 200 mg kg^{-1}) or PBS as control via the tail vein. Behavior observation was carried out for seven days. To further verify *in vivo* toxicity, the mice were sacrificed on the seventh day. Mice's blood were collected by a cardiac puncture method for hematological and were analyzed by blood analyzer (Sysmex XT-1800i, Japan) and Hitachi 7600-110 autoanalyzer (Hitachi, Tokyo, Japan), and the major organs including heart, liver, spleen, lung and kidney were stained with Hematoxylin and Eosin (H&E) and examined by an optical microscope (DMI3000, Leica, Germany).

2.11. In vivo ultrasound-enhanced imaging of BPC-NB-PNBL-NPY

To evaluate the ultrasound-enhanced ability of BPC-NB-PNBL-NPY, Balb/c mice bearing 4T1 cell line tumors were subdivided in two groups, according to the administration route, with 4 animals for intra-tumoral injection and 15 animals for intravenous injection. BPC-NB or BPC-NB-PNBL-NPY suspensions (100 mg kg^{-1}) were injected intravenously through the tail vein or intra-tumorally. For intra-tumoral injection, images were acquired 10, 20, 30, 120, 180 and 300 s after the injection. For intravenous injection, images were acquired approximately 10, 20, 30, 60, 120, 180, 240 and 300 s post injection. The ultrasound transducer was positioned gently on top of the tumor, and the space between them was filled with an adequate
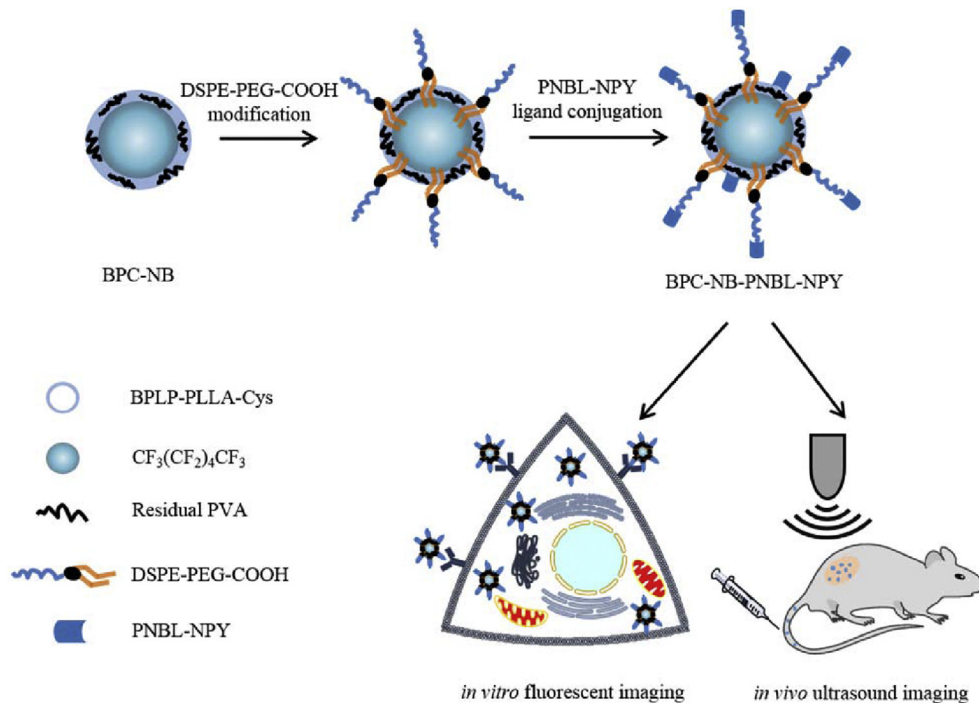
Fig. 1. Schematic illustration of BPC-NB-PNBL-NPY preparation and its application in both *in vitro* fluorescent imaging and *in vivo* ultrasound imaging.

quantity of ultrasonic transmission. A M7 Vet portable ultrasonic imaging system (Mindray, China) was used to perform 2-D imaging of the tumors in the mice, with a 5 MHz probe at a mechanical index of 1.2. The receiver gain and the time gain compensation settings were selected to obtain homogenous brightness throughout the image depth. The dynamic range was 115 dB with a non-linear display curve. After initial selection, these parameters were not changed throughout the series of imaging trials.

2.12. Ex vivo fluorescence imaging

For investigating the biodistribution of the bubbles. Balb/c mice were injected with the same quantity of BPC-NB or BPC-NB-PNBL-NPY via the tail vein. The mice were then sacrificed, and the tumors and major organs were harvested at 0, 3, 10, 30 and 60 min for fluorescence imaging using the Lumina XRMS System. The fluorescence images of the tumors and organs were analyzed via the IVIS Lumina XRMS III (PerkinElmer, USA).

3. Results and discussion

3.1. Preparation and characterization of PNBL-NPY modified BPC-NB

We developed an UCA candidate based on the encapsulation of liquid C_6F_{14} within a biodegradable photoluminescent polymeric

shell through an emulsion-evaporation process derived from the work of Raquel et al. [13]. Afterwards, PNBL-NPY ligands were conjugated to the surface of the BPC-NB (Fig. 1). To improve the amount of PNBL-NPY ligands conjugated, the surface of the BPC-NB was modified with DSPE-PEG-COOH. Due to the biological active site of PNBL-NPY is on the C-terminus, the carboxylic groups of BPC-NB were activated and reacted with the amine groups of PNBL-NPY to protect the biological activity of PNBL-NPY [39]. Different amounts of PNBL-NPY were investigated to check the effect of PNBL-NPY on stability of the prepared NBs (Table 1). Our results indicated that the water solubility and stability of the obtained BPC-NB-PNBL-NPYs were strongly affected by the amount of PNBL-NPY. The mean particle size of the BPC-NB-PNBL-NPY increased from 180.6 to 1472 nm when the amount of PNBL-NPY increased from 0.1 to 1.2 mg. Especially, when the feed ratio of PNBL-NPY to BPC-NB (w/w) was above 100.0 $\mu g\ mg^{-1}$, there was aggregation and precipitation observed. In consideration of the mean size and stability of BPC-NB-PNBL-NPY, 80.0 $\mu g\ mg^{-1}$ of PNBL-NPY to BPC-NB was used for the preparation of BPC-NB-PNBL-NPY, of which the PNBL-NPY conjugation ratio to BPC-NB was 73.6 $\mu g\ mg^{-1}$. TEM indicates that the prepared NBs are spherical in shape and uniform in size, with a mean diameter of ~150 nm (Fig. 2A). Further DLS results show a mean hydrodynamic size of 148.2 nm for BPC-NB and 230.2 nm for BPC-NB-PNBL-NPY, with a narrow size-distribution (polydispersity index (PDI) < 0.285, Fig. 2B and Table 1). As tumors typically exhibit leaky or defective blood vessels, with small

Table 1
Effect of PNBL-NPY ligand amount on conjugation.

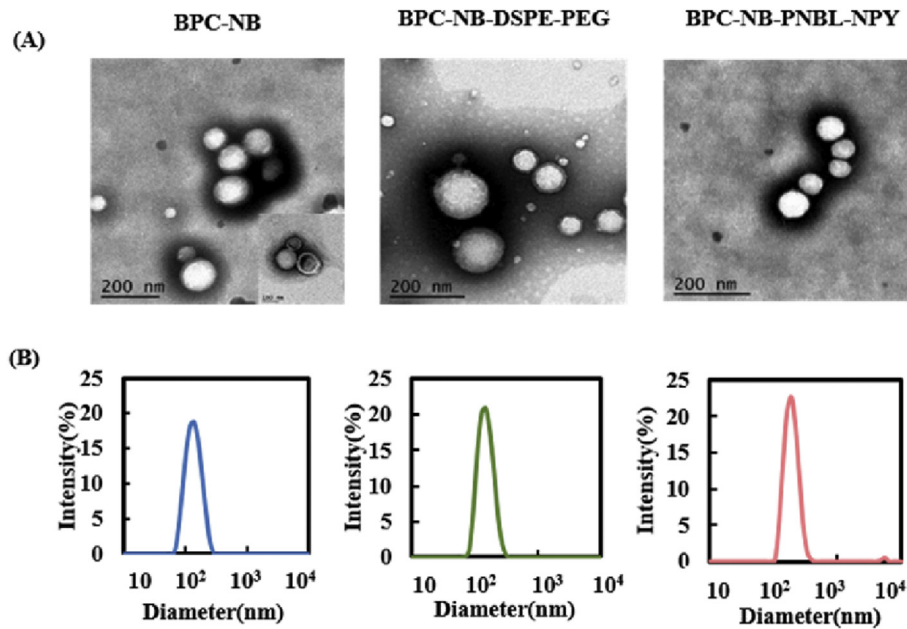| Sample no.	PNBL-NPY (mg)	PNBL-NPY to BPC-NB feed ratio ($\mu g\ mg^{-1}$)	Conjugated PNBL-NPY amounts on surface ($\mu g\ mg^{-1}$)	Reaction ratio	size (nm)	PDI
1	0.0	—	—	—	148.2	0.059
2	0.1	14.3	14.2	99.6%	180.6	0.147
3	0.2	28.6	25.8	90.4%	181.8	0.169
4	0.4	40.0	37.5	93.7%	233.6	0.199
5	0.8	80.0	73.6	91.9%	230.2	0.285
6	1.0	100.0	74.3	74.3%	239.8	0.346
7	1.2	120.0	80.8	67.3%	1472	0.900

Fig. 2. Characterization of BPC-NB-PNBL-NPY. (A) High-resolution transmission electron microscopy (TEM) image of BPC-NB, BPC-NB-DSPE-PEG and BPC-NB-PNBL-NPY. (B) Size distributions of BPC-NB, BPC-NB-DSPE-PEG and BPC-NB-PNBL-NPY in PBS at room temperature measured by dynamic light scattering (DLS) at a scattering angle of 173° (backscatter detection).

pore cutoff sizes up to 780 nm, our prepared NBs were small enough for targeted delivery of nanoparticles to tumor sites [19,40–42]. At pH 7.4, zeta potential values were −5.5 and −3.5 mV for BPC-NB and BPC-NB-PNBL-NPY separately. Although the zeta potential of both NBs were a bit low, but they were stable up to one month at 4 °C, and there was no aggregation observed. The same phenomenon has also been found in the previous literature [13]. After the elimination of surfactants, zeta potential values are close to zero for all the nanocapsules. The change of surface charge might be due to residual PVA present on nanocapsule surface. PVA adsorption arises from hydrogen bonding between PLGA carboxyl groups and PVA hydroxyl groups. In our study, the dispersibility and stability of the colloidal dispersion system were not just depend on the surface charge, but also related to the interfacial energy. Both of the PVA and DSPE-PEG-COOH are excellent surfactant, which can decrease the interfacial energy of the NBs. Moreover, PVA and DSPE-PEG-COOH have hydrophilic groups which can protect the NBs against adsorption between each other in aqueous phase.

The maximum emission and excitation wavelengths of BPLP-PLLA-Cys solution were determined to be 434 and 365 nm, respectively (Fig. S1B). After being incorporated into nanobubbles, the excitation and the emission wavelengths of BPC-NB-PNBL-NPY dislay no significant change (Fig. S2).

3.2. In vitro cell toxicity

The effect of BPC-NB and BPC-NB-PNBL-NPY on the viability of human breast cancer MCF-7 cell line and murine breast cancer 4T1 cell line were investigated after 24 h incubation (Fig. 3). For MCF-7 cells, the cell viability remained above 91.5% for BPC-NB and 93.1% for BPC-NB-PNBL-NPY when the concentrations of NBs varied from 0.2 to 1.0 mg mL^{-1}. For 4T1 cells, the cell viability was above 93.9% for BPC-NB and 89.3% for BPC-NB-PNBL-NPY at all tested concentrations. Compared to the control group, there was about 10.7% cell death induced by BPC-NB-PNBL-NPY. This might be due to the

toxicity of BPC-NBs (about 6%) as well as the PNBL-NPY ligand. In our previous work, we found that the PNBL-NPY ligand itself could inhibit the MCF-7 cell growth in a concentration depend manner, but it has no effect on the normal human breast cells MCF-10A [24]. In the case of 4T1 cells, it might be happened. As both of MCF-7 and 4T1 cells are cancer cells, so this inhibition of cell growth could also be another benefit of our NBs. These results show that both BPC-NB and BPC-NB-PNBL-NPY have good biocompatibility and cause minimal harm to the tested cells.
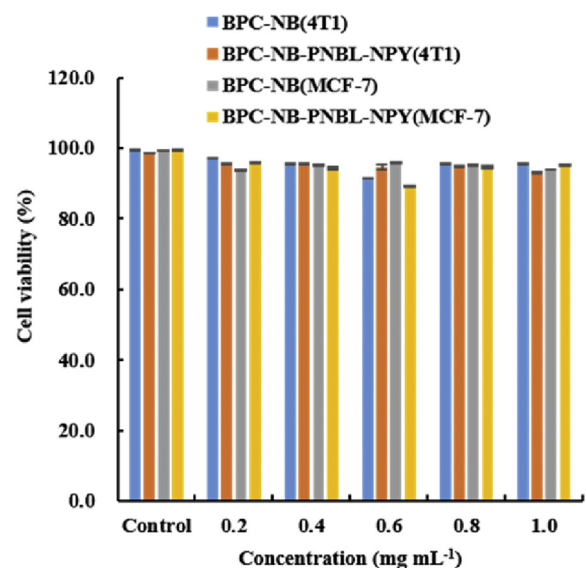

Fig. 3. Cytotoxicity of BPC-NB-PNBL-NPY in MCF-7 cell line of human breast cancer and 4T1 cell line of murine breast cancer. Both MCF-7 and 4T1 cells were treated with different concentration of BPC-NB and BPC-NB-PNBL-NPY for 24 h. Cells were collected and stained by propidium iodide (PI) and analyzed by flow cytometry analysis immediately. Data represent the mean ± SEM (n = 3).
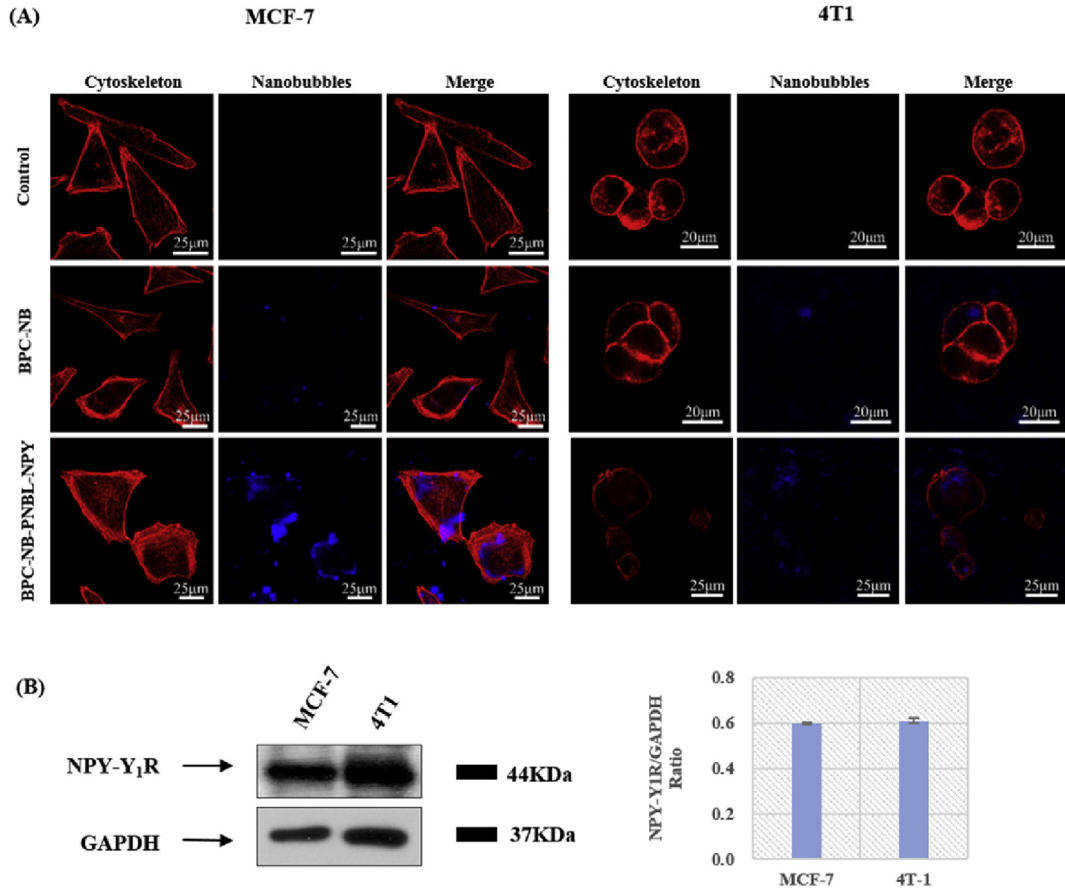
Fig. 4. Cellular uptake of BPC-NB and BPC-NB-PNBL-NPY in MCF-7 and 4T1 cells. (A) Laser scanning confocal microscope (LSCM) images of MCF-7 cells and 4T1 cells incubated with 0.5 mg mL^{-1} BPC-NB and BPC-NB-PNBL-NPY for 12 h. The cytoskeletons with rhodamine phalloidin are red, and the NBs are blue. (B) Western blot analysis of NPY-Y$_1$R expression in MCF-7 cell line of human breast cancer and 4T1 cell line of murine breast cancer. (For interpretation of the references to colour in this figure legend, the reader is referred to the web version of this article.)
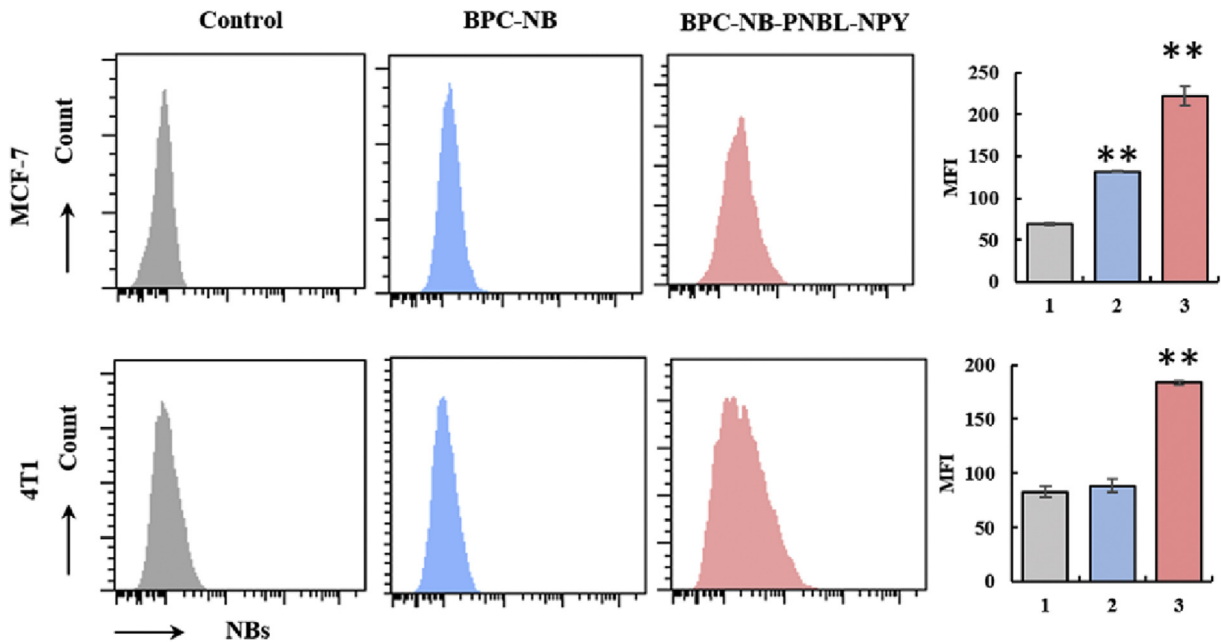
Fig. 5. Flow cytometry analysis of MCF-7 and 4T1 cells incubated with BPC-NB and BPC-NB-PNBL-NPY for 12 h. Significant analysis of mean fluorescence intensity (MFI) for MCF-7 and 4T1 cells incubated with different NBs. Data represent the mean ± SEM (n = 3,*P < 0.05, **P < 0.01). 1: Control; 2: BPC-NB; 3: BPC-NB-PNBL-NPY.

3.3. Cellular uptake of BPC-NB-PNBL-NPY in MCF-7 and 4T1 cells

To evaluate the *in vitro* targeting ability of BPC-NB-PNBL-NPY, cellular uptake of the NBs was assessed using the human breast cancer MCF-7 cell line previously shown to highly express Y_1Rs, and mouse breast cancer 4T1 cell line, which was proven to show a comparable expression rate of Y_1Rs with MCF-7 cells in western blot analysis (Fig. 4B). Both MCF-7 and 4T-1 cells were incubated with BPC-NB and BPC-NB-PNBL-NPY for 12 h, and the LSCM imaging results are shown in Fig. 4A (samples were simultaneously excited at 405 and 540 nm). The cytoskeletons with rhodamine phalloidin (RP) (EX 540 nm, EM 600—660 nm) are red, while the intrinsically fluorescent BPC-NB and BPC-NB-PNBL-NPY (EX 405 nm, EM 420—460 nm) are blue. LSCM images show that PNBL-NPY modified BPC-NB are more internalized into both MCF-7 and 4T1 cells than unmodified BPC-NB. Further flow cytometry analysis (EX 355 nm, EM 425—475 nm) were used to quantify the mean fluorescence intensity (MFI) of NBs treated MCF-7 or 4T1 cells. Fig. 5

shows that the MFI of BPC-NB-PNBL-NPY treated cells are much stronger than BPC-NB, which is 68.1% (P < 0.01) for MCF-7 cells, and 108% (P < 0.01) for 4T1 cells (Fig. 5). Taken together, the above results indicate that PNBL-NPY modification could significantly improve the delivery of BPC-NB into the MCF-7 and 4T1 cells. Our findings agree well with previous reports that PNBL-NPY has the ability to improve internalization of nanoparticles into breast cancer cells [24].

3.4. In vitro ultrasound imaging of BPC-NB-PNBL-NPY

In vitro ultrasonic imaging was performed to confirm the feasibility of the BPC-NB-PNBL-NPY as UCAs. In Fig. 7, it is observed that the latex tube's lumen and wall is very clear before injection of BPC-NB and BPC-NB-PNBL-NPY. After injection, the lumen of the latex tube is brightened for both BPC-NB and BPC-NB-PNBL-NPY. This indicates that our prepared NBs have the potential to act as ultrasound enhanced contrast agents.
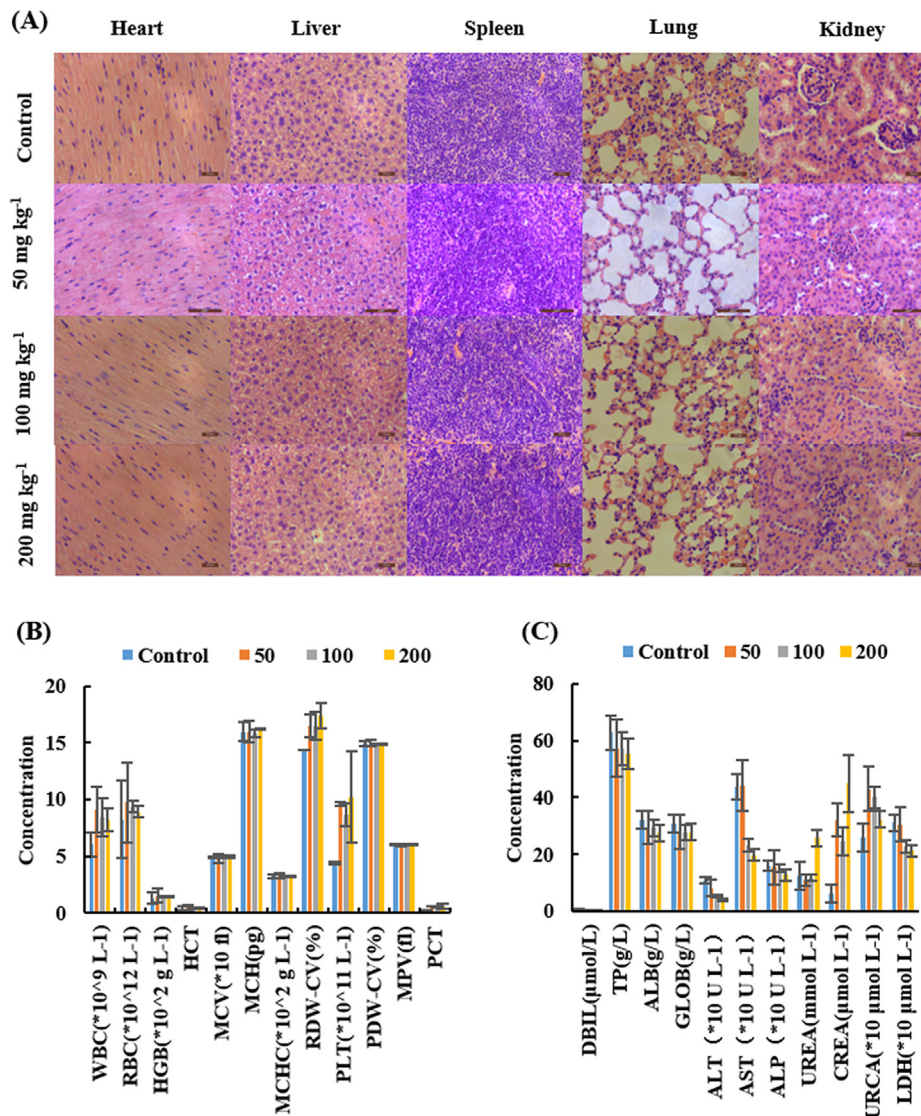

Fig. 6. (A) Histological analysis of mice main organs. Mice were injected intravenously with PBS, 50 mg kg^{-1}, 100 mg kg^{-1} or 200 mg kg^{-1} of BPC-NB-PNBL-NPY and held for seven days. Then the mice were sacrificed and the main organs were collected for the test. (Scale bar = 20 μm).(B) Hematological analysis and (C) blood biochemical analysis of the mice. Data are expressed as the mean ± SEM (n = 3).

3.5. Toxicity evaluation in vivo

As a potential *in vivo* contrast agent, the toxicity of BPC-NB-PNBL-NPY must be evaluated *in vivo*. In this study, histological analysis was used to evaluate the toxicity of the NBs *in vivo* according to previous study. Healthy Blab/c mice were injected intravenously with either PBS, 50, 100 or 200 mg kg^{-1} of BPC-NB-PNBL-NPY. Over a one week period, various behaviors of mice such as eating, drinking, excretion, activity and neurological status were observed. There is no significant difference in the above behaviors between control and BPC-NB-PNBL-NPY groups. After one week, the mice were sacrificed and the main organs were analyzed. Fig. 6 A shows histological analysis of the organs including heart, liver, spleen, lung and kidney. There is no detectable tissue damage or other pathologies such as necrosis, inflammation, or pulmonary fibrosis when comparing the BPC-NB-PNBL-NPY group with the control group. Fig. 6B and C indicates blood analysis and hematological analysis of the mice including white blood cell (WBC), red blood cell (RBC), platelet (PLT), and hemoglobin (HGB), hematocrit (HCT), mean corpuscular volume (MCV), mean corpuscular hemoglobin concentration (MCHC), red blood cell distribution width (RDW-CV), platelet distribution width (PDW-CV), and mean platelet volume (MPV). Number and distribution changes of blood cell are an important indicator of health status. As demonstrated in Fig. 6 B, there is no significant difference between control and different concentrations of BPC-NB-PNBL-NPY groups except PLT, the increase of PLT suggested a possible effect of BPC-NB-PNBL-NPY on blood coagulation, causing damage of platelets. Furthermore, blood biochemical analysis was carried out by blood autoanalyzer. Six important hepatic indicators for liver functions (direct bilirubin, DBIL; albumin, ALB; globin, GLOB; alkaline phosphatase, ALP; gamma glutamyl transpeptidase, GGT), three indicators for kidney functions (urea nitrogen, UREA; creatinine, CREA; uric acid, URCA).

As shown in Fig. 6 C, there is no significant difference between control and different concentrations of BPC-NB-PNBL-NPY groups except AST, UREA and CREA. The decreased AST value indicated the BPC-NB-PNBL-NPY has no effect on the liver function, but the increased UREA and CREA values might suggested the effect of our NBs on the kidney function at the high dose (200 mg kg^{-1}). However, further histological analysis results showed that there was no detectable tissue damage was observed. The pathologist suggested that the changes of UREA and CREA might also because of other unexpected reason, such as the physiological state changes of the mice themselves. In addition, more population need to be collected and analyzed in the future to investigate the detail reason of this phenomenon.

3.6. In vivo ultrasound-enhanced imaging of tumors

In vivo ultrasound imaging was assessed in Balb/c mice bearing 4T1 cell line tumors after either an intra-tumoral or an intravenous injection of BPC-NB or BPC-NB-PNBL-NPY. Fig. 8 presents ultrasound images of tumors before and after the intra-tumoral injection of BPC-NB or BPC-NB-PNBL-NPY. Before injection tumors appear dark whereas after injection tumors present significant contrast enhancement for both types of NBs. The enhancement lasts about 300 s and similar enhancement was observed for all mice included in this trial, but no significant difference could be detected between BPC-NB and BPC-NB-PNBL-NPY.

To evaluate the selective imaging ability of BPC-NB-PNBL-NPY towards breast tumors, an intravenous injection of the NBs was administrated and the imaging characteristics in tumors were analyzed. As shown in Fig. 9A and B, both PNBL-NPY unmodified and modified BPC-NB exhibited ultrasound enhancement ability at tumor sites 30 s after injection. However, the contrast enhancement of BPC-NB-PNBL-NPY (96.4 ± 19.4) was significantly higher
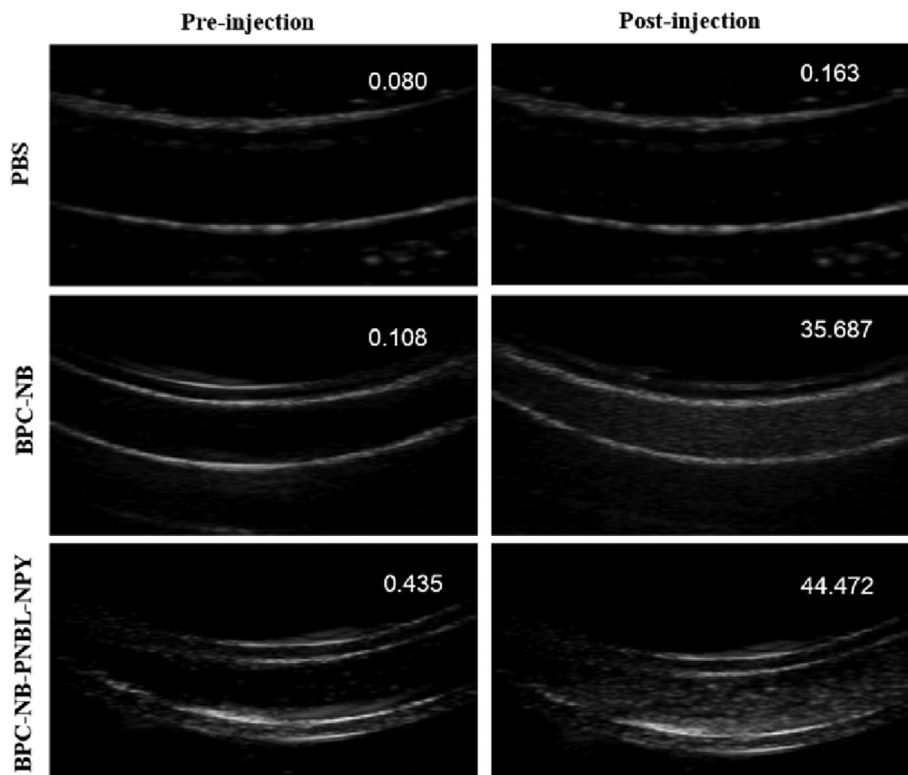

Fig. 7. *In vitro* ultrasound images obtained in a nonlinear imaging mode (THI) at 10 MHz and 10.3 mW cm^{-2} after injection with 5 mL of BP-NB or BP-NB-PNBL-NPY (5 mg mL^{-1}).
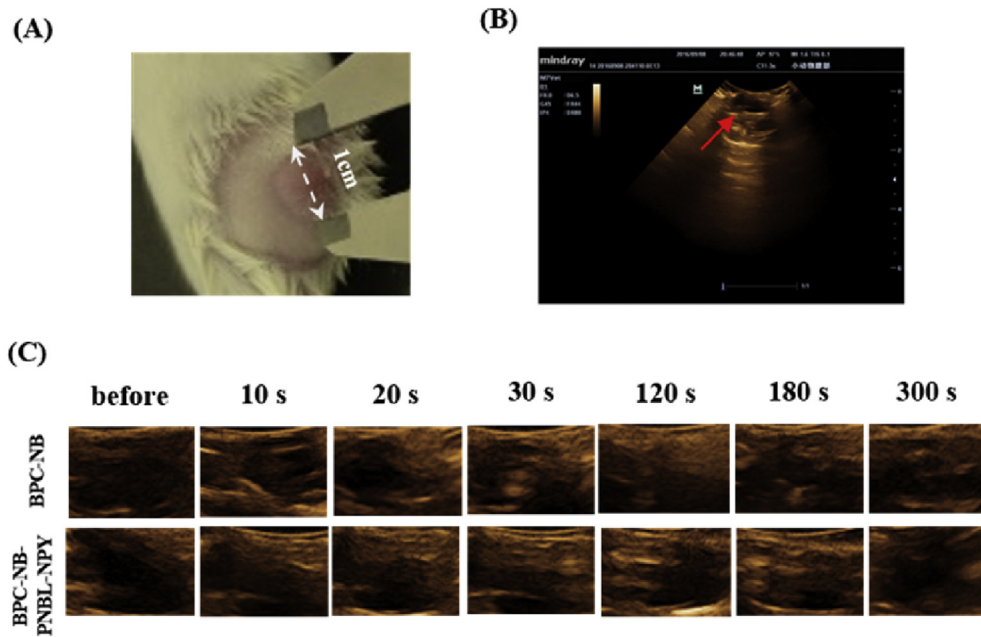
Fig. 8. (A)Y$_1$R-overexpression transplanted tumor in Balb/c mouse model. (B) Conventional ultrasound images of tumor (in red frame). (C) Contrast enhanced ultrasound imaging of tumor before and after intra-tumoral injection of BPC-NB or BPC-NB-PNBL-NPY (100 mg kg^{-1}) at different time points (10, 20, 30, 120, 180 and 300 s). (For interpretation of the references to colour in this figure legend, the reader is referred to the web version of this article.)

than BPC-NB (48.0 ± 10.2) at 30 s after injection (P < 0.05). The enhanced contrast of BPC-NB-PNBL-NPY reached a peak at 60 s (121.6 ± 19.8), and kept in a higher level until 300 s. However, the enhanced contrast of BPC-NB at tumor sites decreased rapidly after 240 s. These findings can be explained by the assumption that the NBs easily passed through the tumor vessels, arrived at the tumor site, or even targeted the Y$_1$Rs in the case of BPC-NB-PNBL-NPY. Additionally, the contrast enhancement of NBs could also be observed in the background around tumors from 30 to 120 s. This might be due to the increased circulation of NBs in the blood vessels
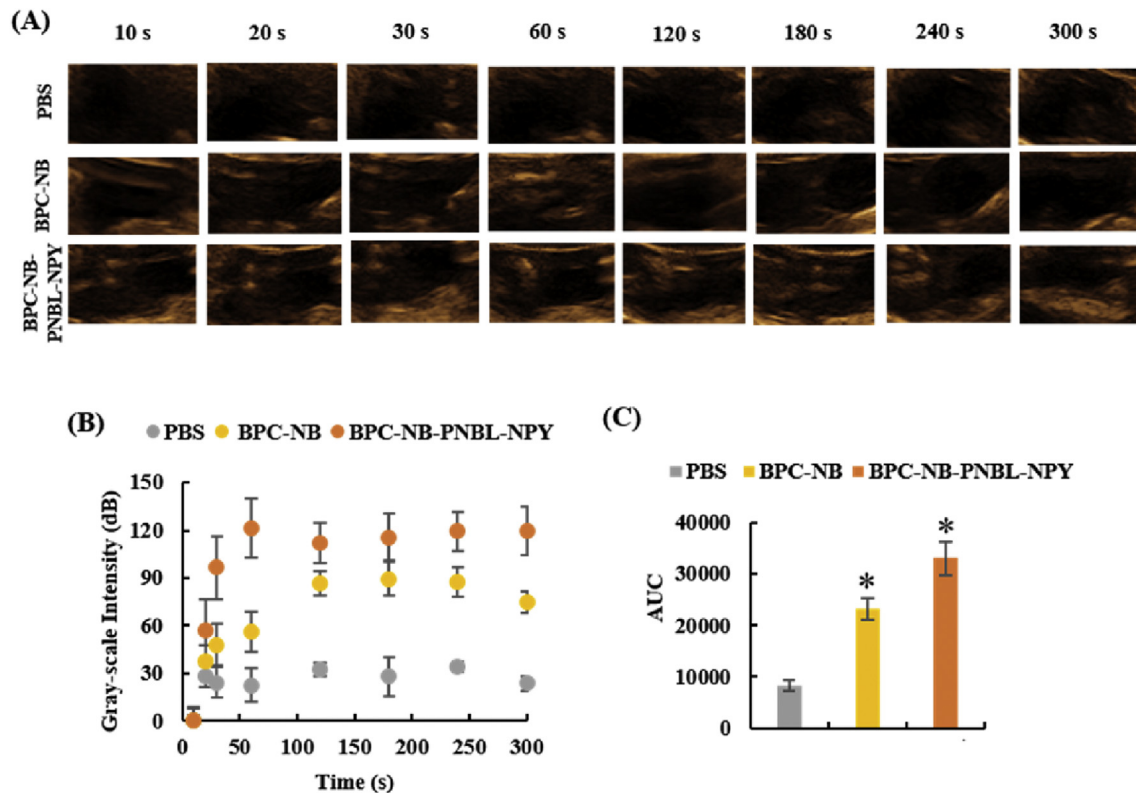

Fig. 9. *In vivo* ultrasound-enhanced imaging of BPC-NB-PNBL-NPY. (A) Contrast enhanced ultrasound imaging of tumor after intravenous injection of PBS, BPC-NB or BPC-NB-PNBL-NPY (100 mg kg^{-1}) at different time points (10, 20, 30, 60, 120, 180, 240 and 300 s). (B and C) Time-gray scale intensity curves and AUC analysis. Data represent the mean ± SEM (n = 3,*P < 0.05, **P < 0.01).
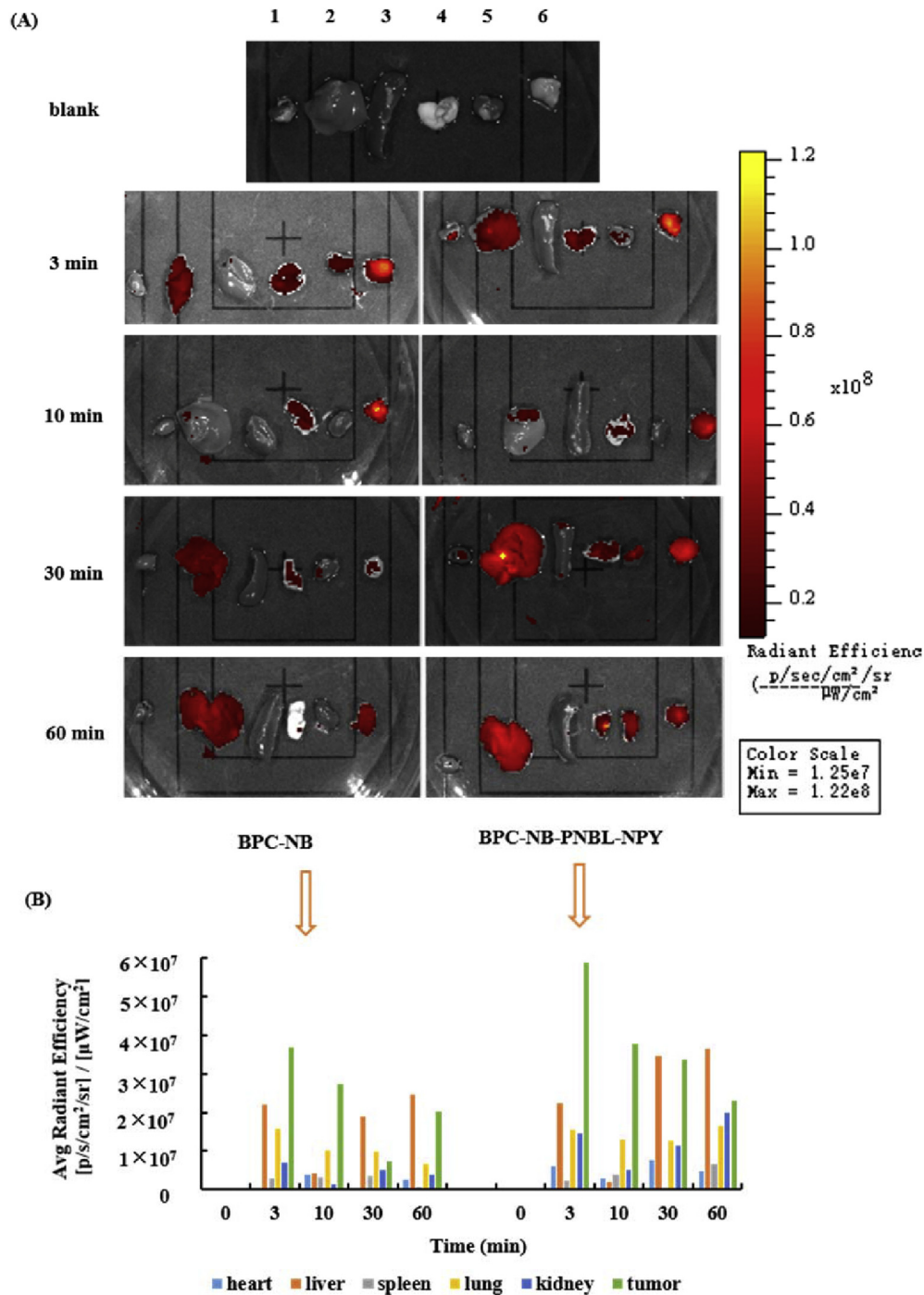
Fig. 10. (A) *Ex vivo* fluorescence imaging results for BPC-NB and BPC-NB-PNBL-NPY group at 0, 3, 10, 30 and 60min. In each image: 1. heart; 2. liver; 3. spleen; 4. lung; 5. kidney; 6. tumor. (B) ROI analysis of heart, liver, spleen, spleen, kidney and tumor in *ex vivo* fluorescence imaging for the two groups at 0, 3, 10, 30 and 60 min.

around tumors. After 300 s, the enhanced background signal decreased slowly, while the contrast enhancement of BPC-NB-PNBL-NPY could still be observed at the tumor sites. This might be due to the selective targeting of BPC-NB-PNBL-NPY on the Y_1Rs of tumors, while the NBs in the blood vessels around the tumor tissues were cleared away quickly. To further compare the contrast enhancement of the NBs as a function of imaging time, area under the curve (AUC) plots from 10 to 300 s were analyzed by Phoenix WinNonlin 6.4 software (Certara, USA). In Fig. 9C, it indicated that enhancements induced by the BPC-NB-PNBL-NPY (AUC: 33,121 ± 3046) were significantly stronger than the enhancement

induced by the BPC-NB (AUC: 23,315 ± 2089) (P < 0.05). These results suggest that PNBL-NPY modified BPC-NB can more easily arrive at tumors, pass through the tumor capillaries and target Y_1R-overexpressing tumor cells. The high affinity between PNBL-NPY and Y_1Rs on tumor cells allows more BPC-NB-PNBL-NPY to remain at the tumor site and coalesce to form MBs, which exhibit a higher scattering cross-section than that of BPC-NB and produce superior contrast enhancement [19,43].

In previous studies, NBs with different formulations demonstrated excellent ultrasound imaging enhancement *in vivo*. Histological examination has demonstrated that NBs can pass through

the endothelial gaps of tumors. These results have been attributed to EPR effects [15,44,45]. However, most cases of the EPR effects of NBs have previously been correlated with poor *in vivo* tumor selectivity during intravenous delivery [13,15]. For example, NBs prepared by Raquel et al. produced extensive and strong ultrasound imaging enhancement by intra-tumoral injection but cannot be detected by intravenous injection [13]. The typical solution employed to achieve tumor selectivity is to conjugate specific targeted molecules (such as ligands or antibodies) to the surface of NBs, which can target to specific receptors or antigens expressed on the tumors [15,19,46,47]. For example, NBs-affibody has been prepared for human epidermal growth factor receptor type 2 (HRE2)-targeted ultrasound imaging, providing good ultrasound-enhanced signal [19]. Although the affibody was able to mimic the function of an antibody with a low molecular weight of 14 kDa, it was still composed of 58 amino acid residues. However, the PNBL-NPY ligand that we used here only consists of 9 amino acids, which might provide higher labeling efficiency with a lower synthesis cost compared to large peptides [48,49]. In addition, the size of BPC-NB-PNBL-NPY (~230 nm) was much smaller than the NBs-affibody (~478 nm), but still displayed good ultrasound enhancement. Moreover, due to the use of photoluminescent polymers, our fluorescent BPC-NBs could also be explored for photoacoustic imaging of tumors in the future [50,51]. Therefore, the PNBL-NPY modified NBs may provide an alternative in the early diagnosis and treatment of Y_1R-overexpressing breast cancers.

3.7. Ex vivo fluorescence imaging

To further confirm the targeted selectivity of BPC-NB-PNBL-NPY toward tumors, we performed *ex vivo* fluorescence imaging experiments. The fluorescence signal intensity of *ex vivo* imaging is a reflection of the BPC-NB-PNBL-NPY retained inside the organs because of the low or even lack of autofluorescence observed in *ex vivo* images [52]. Tumors and major organs from the mice injected with the BPC-NB or BPC-NB-PNBL-NPY groups were harvested to acquire fluorescence images at different time points. As shown in Fig. 10A, the fluorescence was obviously distributed in the tumors, livers and kidneys, but less fluorescence signal was detected in hearts and spleens. A region of interest (ROI) analysis were performed on the *ex vivo* fluorescence images to semi-quantitatively analyze the DiI uptake in each organs. Fig. 10B indicated that the BPC-NB-PNBL-NPY induced fluorescence in tumors were much higher than the BPC-NBs after the injection 3 min (5.9×10^7 vs 3.7×10^7) to 60 min (2.3×10^7 vs 2.0×10^7). These results confirmed that the targeted selectivity of BPC-NB-PNBL-NPY was distinct at 3 min after intravenous injection, which was consistent with the results of *in vivo* ultrasound imaging. Taken together, the *ex vivo* imaging results further confirmed the targetability of BPC-NB-PNBL-NPY to Y_1Rs-over expressing tumors.

4. Conclusion

In this work, we have developed Y_1R-based biodegradable photoluminescent NBs as UCAs with excellent dispersibility, stability and biocompatibility. The hydrodynamic size of our BPC-NB-PNBL-NPY could be under 240 nm in diameter, favoring extravasation. The *in vitro* fluorescence spectra and CLSM experiment show that the BPC-NB-PNBL-NPY exhibits bright and stable autofluorescence, facilitating tracking of their interaction with various cells. Further, we demonstrated that the BPC-NB-PNBL-NPY exhibits high affinity and specificity to Y_1R-overexpressing breast cancer cells and tumors, decreasing toxicity while providing good ultrasound enhancement in both *in vitro* and *in vivo* experiments. These results indicate that the fabricated Y_1R-based NBs have the

potential to be excellent UCAs in Y_1R positive breast cancer imaging and might also provide a potential nanoplatform for Y_1R positive breast cancer treatment.

Appendix A. Supplementary data

Supplementary data related to this article can be found at http://dx.doi.org/10.1016/j.biomaterials.2016.11.028.

References

[1] L.A. Torre, F. Bray, R.L. Siegel, J. Ferlay, J. Lortet-Tieulent, A. Jemal, Global cancer statistics, 2012, CA Cancer J. Clin. 65 (2015) 87—108.
[2] M.A. Richards, The national awareness and early diagnosis initiative in England: assembling the evidence introduction, Br. J. Cancer 101 (2009) S1—S4.
[3] M.P. Coleman, D. Forman, H. Bryant, J. Butler, B. Rachet, C. Maringe, et al., Cancer survival in Australia, Canada, Denmark, Norway, Sweden, and the UK, 1995-2007 (the international cancer benchmarking partnership): an analysis of population-based cancer registry data, Lancet 377 (2011) 127—138.
[4] R. Weissleder, Molecular imaging in cancer, Science 312 (2006) 1168—1171.
[5] S.R. Wilson, P.N. Burns, Microbubble-enhanced US in body imaging: what role? Radiology 257 (2010) 24—39.
[6] F. Kiessling, S. Fokong, P. Koczera, W. Lederle, T. Lammers, Ultrasound microbubbles for molecular diagnosis, therapy, and theranostics, J. Nucl. Med. 53 (2012) 345—348.
[7] V. Sanna, G. Pintus, P. Bandiera, R. Anedda, S. Punzoni, B. Sanna, et al., Development of polymeric microbubbles targeted to prostate-specific membrane antigen as prototype of novel ultrasound contrast agents, Mol. Pharm. 8 (2011) 748—757.
[8] S. Hernot, A.L. Klibanov, Microbubbles in ultrasound-triggered drug and gene delivery, Adv. Drug Deliv. Rev. 60 (2008) 1153—1166.
[9] K.W. Ferrara, M.A. Borden, H. Zhang, Lipid-shelled vehicles: engineering for ultrasound molecular imaging and drug delivery, Acc. Chem. Res. 42 (2009) 881—892.
[10] A. Gong, X.H. Ma, L.C. Xiang, W.Z. Ren, Z.Y. Shen, A.G. Wu, Improved double emulsion technology for fabricating autofluorescent microcapsules as novel ultrasonic/fluorescent dual-modality contrast agents, Colloid Surf. B 116 (2014) 561—567.
[11] E. Pisani, E. Fattal, J. Paris, C. Ringard, V. Rosilio, N. Tsapis, Surfactant dependent morphology of polymeric capsules of perfluorooctyl bromide: influence of polymer adsorption at the dichloromethane-water interface, J. Colloid Interf. Sci. 326 (2008) 66—71.
[12] E. Pisani, N. Tsapis, J. Paris, V. Nicolas, L. Cattel, E. Fattal, Polymeric nano/microcapsules of liquid perfluorocarbons for ultrasonic imaging: physical characterization, Langmuir 22 (2006) 4397—4402.
[13] R. Díaz-López, N. Tsapis, M. Santin, S.L. Bridal, V. Nicolas, D. Jaillard, et al., The performance of PEGylated nanocapsules of perfluorooctyl bromide as an ultrasound contrast agent, Biomaterials 31 (2010) 1723—1731.
[14] J.S. Xu, J.W. Huang, R.G. Qin, G.H. Hinkle, S.P. Povoski, E.W. Martin, et al., Synthesizing and binding dual-mode poly (lactic-co-glycolic acid) (PLGA) nanobubbles for cancer targeting and imaging, Biomaterials 31 (2010) 1716—1722.
[15] T.H. Yin, P. Wang, R.Q. Zheng, B.W. Zheng, D. Cheng, X.L. Zhang, et al., Nanobubbles for enhanced ultrasound imaging of tumors, Int. J. Nanomed. 7 (2012) 895—904.
[16] N. Rapoport, Z.G. Gao, A. Kennedy, Multifunctional nanoparticles for combining ultrasonic tumor imaging and targeted chemotherapy, J. Natl. Cancer Inst. 99 (2007) 1095—1106.

[17] I.U. Khan, A.G. Beck-Sickinger, Targeted tumor diagnosis and therapy with peptide hormones as radiopharmaceuticals, Anti Cancer Agents Med. Chem. 8 (2008) 186—199.

[18] K. Temming, R.M. Schiffelers, G. Molema, R.J. Kok, RGD-based strategies for selective delivery of therapeutics and imaging agents to the tumour vasculature, Drug Resist. Update 8 (2005) 381—402.

[19] H.L. Yang, W.B. Cai, L. Xu, X.H. Lv, Y.B. Qiao, P. Li, et al., Nanobubble-Affibody: novel ultrasound contrast agents for targeted molecular ultrasound imaging of tumor, Biomaterials 37 (2015) 279—288.

[20] W. Xia, P.S. Low, Folate-targeted therapies for Cancer, J. Med. Chem. 53 (2010) 6811—6824.

[21] Q. Chen, H.J. Millar, F.L. McCabe, C.D. Manning, R. Steeves, K. Lai, et al., Alphav integrin-targeted immunoconjugates regress established human tumors in xenograft models, Clin. Cancer Res. Off. J. Am. Assoc. Cancer Res. 13 (2007) 3689—3695.

[22] J.C. Reubi, U. Läderach, B. Waser, J.-O. Gebbers, P. Robberecht, J.A. Laissue, Vasoactive intestinal peptide/pituitary adenylate cyclase-activating peptide receptor subtypes in human tumors and their tissues of origin, Cancer Res. 60 (2000) 3105—3112.

[23] M. Gugger, J.C. Reubi, Gastrin-releasing peptide receptors in non-neoplastic and neoplastic human breast, Am. J. Pathol. 155 (1999) 2067—2076.

[24] J. Li, Z.Y. Shen, X.H. Ma, W.Z. Ren, L.C. Xiang, A. Gong, et al., Neuropeptide Y Y-1 receptors mediate targeted delivery of anticancer drug with encapsulated nanoparticles to breast Cancer cells with high selectivity and its potential for breast Cancer therapy, ACS Appl. Mater. Interfaces 7 (2015) 5574—5582.

[25] M. Körner, J.C. Reubi, NPY receptors in human cancer: a review of current knowledge, Peptides 28 (2007) 419—425.

[26] J.C. Reubi, M. Gugger, B. Waser, J.C. Schaer, Y-1-mediated effect of neuropeptide Y in cancer: breast carcinomas as targets, Cancer Res. 61 (2001) 4636—4641.

[27] S. Hofmann, S. Maschauer, T. Kuwert, A.G. Beck-Sickinger, O. Prante, Synthesis and in vitro and in vivo evaluation of an (18)F-Labeled neuropeptide Y analogue for imaging of breast Cancer by PET, Mol. Pharm. 12 (2015) 1121—1130.

[28] N. Braekeveldt, C. Wigerup, D. Gisselsson, S. Mohlin, M. Merselius, S. Beckman, et al., Neuroblastoma patient-derived orthotopic xenografts retain metastatic patterns and geno- and phenotypes of patient tumours, Int. J. Cancer 136 (2015) E252—E261.

[29] C. Morgat, A.K. Mishra, R. Varshney, M. Allard, P. Fernandez, E. Hindie, Targeting neuropeptide receptors for Cancer imaging and therapy: perspectives with bombesin, neurotensin, and Neuropeptide-Y receptors, J. Nucl. Med. 55 (2014) 1650—1657.

[30] M. Memminger, M. Keller, M. Lopuch, N. Pop, G. Bernhardt, E. von Angerer, et al., The neuropeptide Y Y-1 receptor: a diagnostic Marker? Expression in MCF-7 breast Cancer cells is down-regulated by antiestrogens in vitro and in xenografts, PLoS One 7 (2012) 11.

[31] I.U. Khan, D. Zwanziger, I. Bohme, M. Javed, H. Naseer, S.W. Hyder, et al., Breast-Cancer diagnosis by neuropeptide Y analogues: from synthesis to clinical application, Angew. Chem Int Ed. 49 (2010) 1155—1158.

[32] D. Gyawali, S.Y. Zhou, R.T. Tran, Y. Zhang, C. Liu, X.C. Bai, et al., Fluorescence imaging enabled biodegradable photostable polymeric micelles, Adv. Healthc. Mater. 3 (2014) 182—186.

[33] J. Yang, Y. Zhang, S. Gautam, L. Liu, J. Dey, W. Chen, et al., Development of aliphatic biodegradable photoluminescent polymers, Proc. Natl. Acad. Sci. U. S. A. 106 (2009) 10086, 2009;106:11818.

[34] Z.W. Xie, Y. Zhang, L. Liu, H. Weng, R.P. Mason, L.P. Tang, et al., Development of intrinsically photoluminescent and photostable polylactones, Adv. Mater. 26 (2014) 4491—4496.

[35] A.S. Wadajkar, T. Kadapure, Y. Zhang, W.N. Cui, K.T. Nguyen, J. Yang, Dual-imaging enabled Cancer-Targeting nanoparticles, Adv. Health. Mater. 1 (2012) 450—456.

[36] J. Hu, J. Guo, Z. Xie, D. Shan, E. Gerhard, G. Qian, et al., Fluorescence imaging enabled poly(lactide-co-glycolide), Acta Biomater. 29 (2016) 307—319.

[37] G.J. Chen, L.W. Wang, T. Cordie, C. Vokoun, K.W. Eliceiri, S.Q. Gong, Multi-functional self-fluorescent unimolecular micelles for tumor-targeted drug delivery and bioimaging, Biomaterials 47 (2015) 41—50.

[38] J. Fan, Y. Sun, S. Wang, Y. Li, X. Zeng, Z. Cao, et al., Inhibition of autophagy overcomes the nanotoxicity elicited by cadmium-based quantum dots, Biomaterials 78 (2016) 102—114.

[39] I. Böhme, J. Stichel, C. Walther, K. Mörl, A.G. Beck-Sickinger, Agonist induced receptor internalization of neuropeptide Y receptor subtypes depends on third intracellular loop and C-terminus, Cell. Signal. 20 (2008) 1740—1749.

[40] J. Kim, Y.M. Lee, Y. Kang, W.J. Kim, Tumor-homing, size-tunable clustered nanoparticles for anticancer therapeutics, Acs Nano 8 (2014) 9358—9367.

[41] A. Albanese, P.S. Tang, W.C.W. Chan, The effect of nanoparticle size, shape, and surface chemistry on biological systems, Annu. Rev. Biomed. Eng. 14 (2012) 1—16.

[42] H. Kim, D. Lee, J. Kim, T.I. Kim, W.J. Kim, Photothermally triggered cytosolic drug delivery via endosome disruption using a functionalized reduced graphene oxide, Acs Nano 7 (2013) 6735—6746.

[43] N. Deshpande, A. Needles, J.K. Willmann, Molecular ultrasound imaging: current status and future directions, Clin. Radiol. 65 (2010) 567—581.

[44] H.-P. Tong, L.-F. Wang, Y.-L. Guo, L. Li, X.-Z. Fan, J. Ding, et al., Preparation of protamine cationic nanobubbles and experimental study of their physical properties and in vivo contrast enhancement, Ultrasound Med. Biol. 39 (2013) 2147—2157.

[45] H. Wu, N.G. Rognin, T.M. Krupka, L. Solorio, H. Yoshiara, G. Guenette, et al., Acoustic characterization and pharmacokinetic analyses of new nanobubble ultrasound contrast agents, Ultrasound Med. Biol. 39 (2013) 2137—2146.

[46] S.M. Stieger, P.A. Dayton, M.A. Borden, C.F. Caskey, S.M. Griffey, E.R. Wisner, et al., Imaging of angiogenesis using Cadence™ contrast pulse sequencing and targeted contrast agents, Contrast Media Mol. Imaging 3 (2008) 9—18.

[47] G.E.R. Weller, M.K.K. Wong, R.A. Modzelewski, E.X. Lu, A.L. Klibanov, W.R. Wagner, et al., Ultrasonic imaging of tumor angiogenesis using contrast microbubbles targeted via the tumor-binding peptide arginine-arginine-leucine, Cancer Res. 65 (2005) 533—539.

[48] D. Zwanziger, I. Bohme, D. Lindner, A.G. Beck-Sickinger, First selective agonist of the neuropeptide Y-1-receptor with reduced size, J. Pept. Sci. 15 (2009) 856—866.

[49] J. Li, Y. Tian, A. Wu, Neuropeptide Y receptors: a promising target for cancer imaging and therapy, Regen. Biomater. 2 (2015) 215—219.

[50] X.D. Wang, Y.J. Pang, G. Ku, X.Y. Xie, G. Stoica, L.H.V. Wang, Noninvasive laser-induced photoacoustic tomography for structural and functional in vivo imaging of the brain, Nat. Biotechnol. 21 (2003) 803—806.

[51] H.F. Zhang, K. Maslov, G. Stoica, L.H.V. Wang, Functional photoacoustic microscopy for high-resolution and noninvasive in vivo imaging, Nat. Biotechnol. 24 (2006) 848—851.

[52] J. Gao, K. Chen, R. Xie, J. Xie, Y. Yan, Z. Cheng, et al., In vivo tumor-targeted fluorescence imaging using near-infrared non-cadmium quantum dots, Bioconjug. Chem. 21 (2010) 604—609.